36th AIAA Fluid Dynamics Conference and Exhibit
5 - 8 June 2006, San Francisco, California

AIAA 2006-3360

Unsteady Phenomena in Supersonic Nozzle Flow Separation

Dimitri Papamoschou* and Andrew Johnson†
University of California, Irvine, Irvine, CA 92697-3975

This work considers the instability of the jet plume from an overexpanded, shock-containing convergent-divergent nozzle and attempts to correlate this instability to internal shock-induced separation phenomena. Time resolved wall pressure measurements and Pitot measurements are used as primary diagnostics. For the conditions of this study flow separation is asymmetric resulting in a large separation zone on one wall and a small separation zone on the other wall. Correlations of wall pressures indicate a low-frequency, piston-like shock motion without any resonant tones. Correlations of Pitot pressure with wall pressures indicate strong coherence of shear-layer instability with the shock motion. The likely source of the plume instability is the interaction of unsteady waves generated past the main separation shock with the shear layer of the large separation region.

Nomenclature

A	=	cross sectional area
C	=	coherence
f	=	frequency
h	=	nozzle height
NPR	=	nozzle pressure ratio=p_{res}/p_a
p	=	pressure
R	=	normalized correlation
S	=	spectrum
U	=	velocity
σ	=	standard deviation

Subscripts

a	=	ambient
e	=	exit
o	=	total
res	=	reservoir
rms	=	root mean square
t	=	throat
1	=	lower wall transducer
2	=	upper wall transducer
3	=	dynamic Pitot probe

I. Introduction

Supersonic flow separation in a convergent-divergent nozzle results in instability of the plume exiting the nozzle. This can be used to enhance mixing of the nozzle flow. Alternatively, the instability can be used as an excitation means to destabilize a flow adjacent to the nozzle. Potential applications include fuel injection, ejectors, and thermal signature reduction from jet engines. The instability phenomenon was initially observed in coannular jet experiments at the University of California, Irvine[1], where an arbitrary primary jet surrounded by a secondary jet from a convergent-divergent nozzle showed substantial improvements in mixing compared to the case where the secondary nozzle was simply convergent. Figure 1 presents a visual example of such instability. This method has

* Professor, Department of Mechanical and Aerospace Engineering, 4200 Engineering Gateway, Irvine, CA 92697-3975, AIAA Associate Fellow.
† Graduate Student Researcher, Department of Mechanical and Aerospace Engineering, 4200 Engineering Gateway, Irvine, CA 92697-3975, AIAA Member.

accordingly been named Mixing Enhancement via Secondary Parallel Injection (MESPI). It has been investigated in round and rectangular jets at UCI[1-3], and in larger-scale round jets at NASA Glenn Research Center[4]. A typical result is that the length of the potential core is reduced by 50% and the velocity past the potential core decays at a much faster rate than for the equivalent jet without MESPI. For a nozzle with a given expansion ratio, the range of nozzle pressure ratios over which the instability occurs coincides with the range of nozzle pressure ratios for which a shock was located inside the nozzle. Therefore, the phenomenon of supersonic nozzle flow separation was deemed responsible for the observed instability.

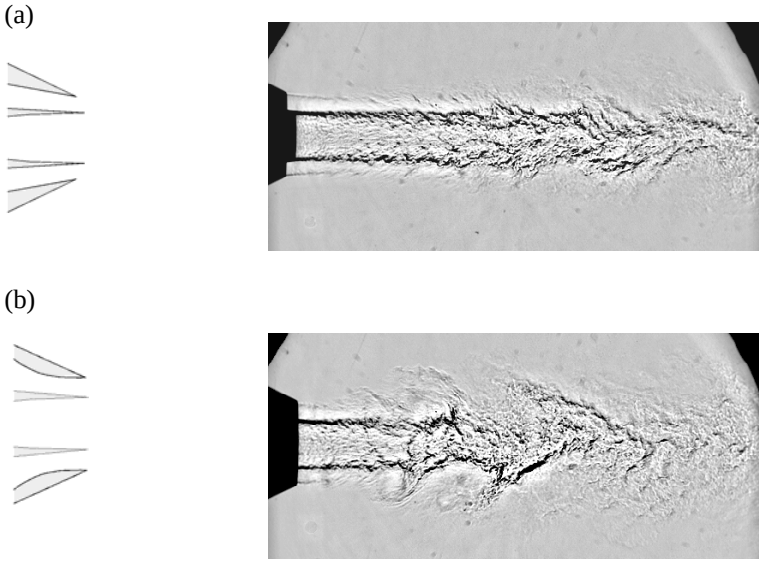

Fig.1 Primary jet flow at Mach 0.9 surrounded by an annular secondary flow at nozzle pressure ratio NPR=1.7 (a) Secondary nozzle is convergent; (b) secondary nozzle is convergent-divergent.

Numerous past studies have investigated supersonic nozzle flow separation[5-9], but their focus was on the internal flow phenomena and not so much on the unstable plume that emerges from the separation shock. A related effort has focused on the phenomenon of transonic resonance in convergent-divergent nozzles[10]. Transonic resonance appears to occur in relatively small nozzles where the boundary layer before the shock is laminar. For large nozzles with a turbulent boundary layer, such as those investigated here, there is no evidence of resonant phenomena.

To better understand the phenomenon of nozzle flow separation and its connection to flow instability, a fundamental experimental effort was started at UCI using a specially designed facility, to be described later in this report. Figure 2 shows a picture of nozzle flow separation obtained in this facility[11]. As is evident from the photograph, the phenomenon is very complex and much more intricate than one would expect from quasi-one dimensional theory. The illustration of Fig.3 highlights some key features of the flow, but it is by no means complete.

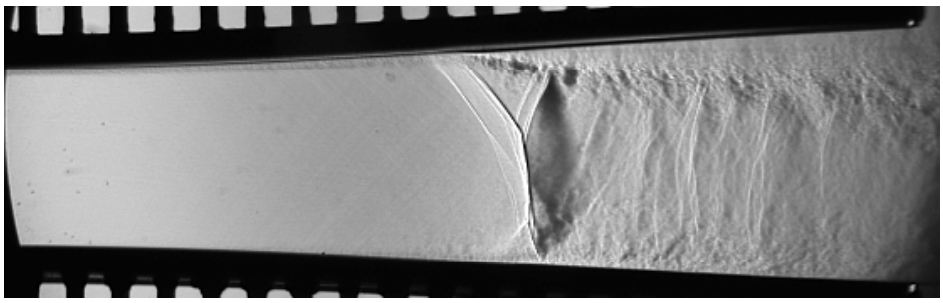

Fig.2 Spark schlieren image of supersonic nozzle flow separation. From Ref. 11

The shock in the viscous case takes on a bifurcated structure consisting of an incident shock and a reflected shock merging into a Mach stem. This is commonly referred to as a lambda foot, and the point at which the three components meet is called the triple point. The Mach stem is essentially a normal shock producing subsonic outflow. For the range of conditions of interest here, the incident and reflected shocks are of the "weak" type resulting in supersonic outflow past both. The adverse pressure gradient of the incident shock causes the boundary layer to separate and detach from the wall as a shear layer that bounds the separation (recirculation) region. Emerging from the triple point is a slipstream forming a sonic throat that acts to reaccelerate the subsonic region. The reflected portion of the main shock structure will then emerge from the separation shear layer as an expansion fan that is then transmitted through the slipstream toward the other separation shear layer where it is reflected again into compression waves, this pattern repeating with downstream distance. Therefore the separation "jet" that emerges from the shock contains a series of alternating compression and expansion waves.

In nozzles with straight or convex walls subjected to nozzle pressure ratios above about 1.4, separation is asymmetric wherein one lambda foot is larger than the other (see for example Fig.2). The asymmetry does not flip during an experiment but may change sides from one experiment to the next. A recent computational effort by Xiao et al.[12] also predicted asymmetric separation. This asymmetry has been recognized as a key factor for mixing enhancement. Papamoschou and Zill[11] discovered large eddies forming in the shear layer of the large separation region, sometimes occupying over half the test section height. It was suspected that these eddies were due to the unsteady nature of the main shock. The objective of this paper is to investigate possible connections between the oscillation of the main shock and the occurrence of large-scale turbulent fluctuations downstream of the shock.

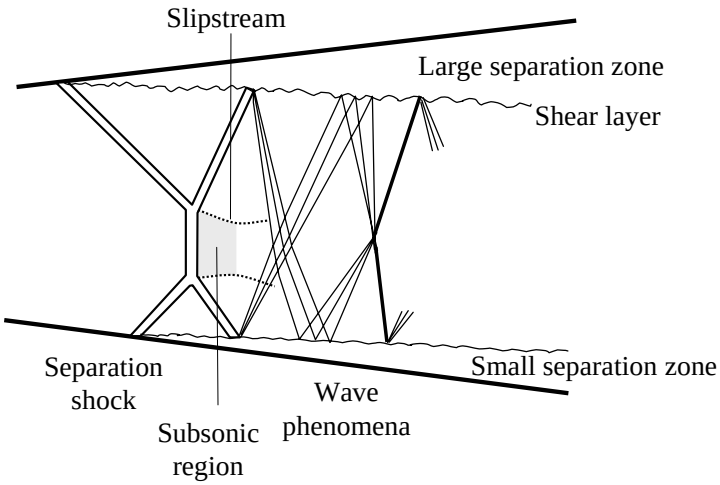

Fig.3 Schematic of principal phenomena of supersonic nozzle flow separation

II. Experimental Setup

A. Flow Facility

The experiments used a facility designed specifically for studying flow separation in nozzles of various shapes[11], shown in Fig.4. The nozzle apparatus consists of two flexible plates that can be shaped using two sets of actuators to form the upper and lower walls. One set of actuators controls the transverse force applied to the plates and the other controls the moment applied, allowing variations in nozzle area ratio, nozzle contour and exit angle. The nominal test section dimensions are 22.9 mm in height, 63.5 mm in width, and 117 mm in length from throat to exit. The sidewalls of the nozzle incorporate large optical windows for visualization of the entire internal flow, from the subsonic converging section to the nozzle exit. The apparatus is connected to a system of pressure-regulated air capable of nozzle pressure ratios as high as 3.5.

The nozzle pressure ratio (NPR) ranged from 1.2 to 1.8 resulting in ideally-expanded velocities U_e ranging from 170 m/s to 320 m/s. The Reynolds number prior to the shock, based on axial distance from the throat, was typically 2.5×10^6. This indicates a fully-turbulent boundary layer.

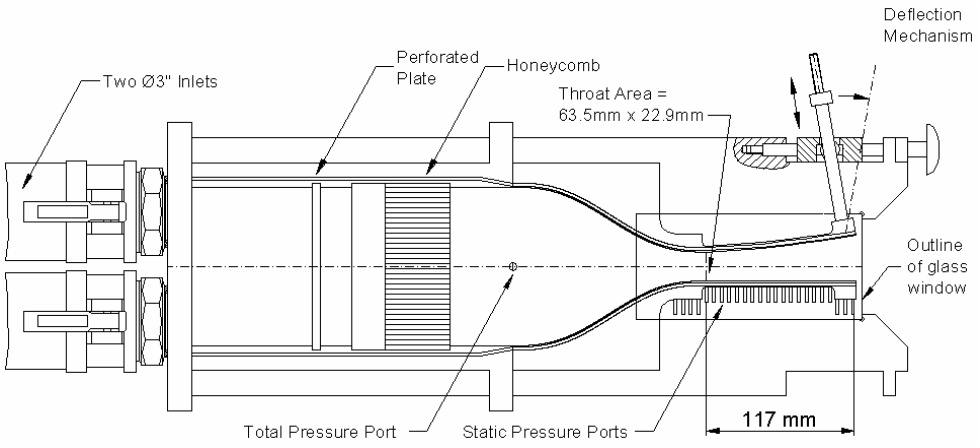

Fig.4 Rectangular nozzle apparatus

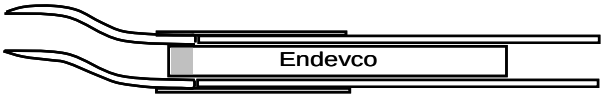

Fig.5 Design of dynamic Pitot probe (DPP)

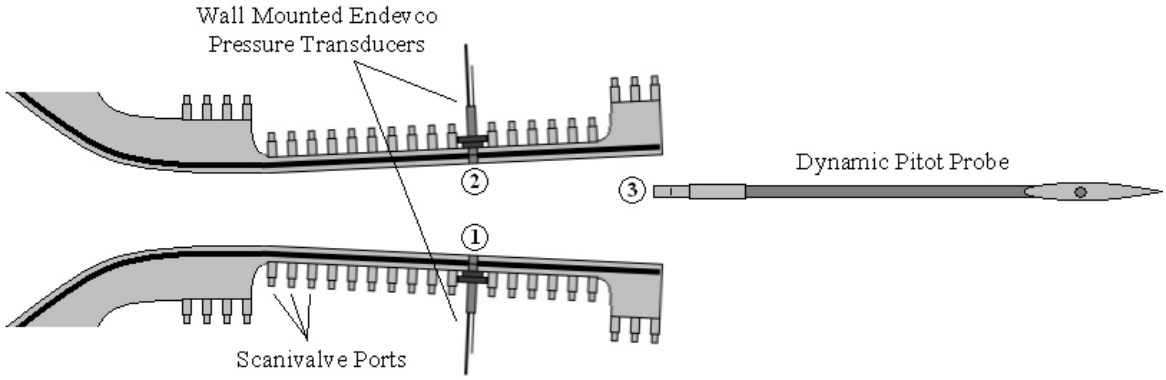

Fig.6 Location of wall transducers and one of the positions of the dynamic Pitot probe

B. Instrumentation

It was evident from previous experiments that there was a clear need for time resolved measurements of the static pressure on the nozzle walls. Accordingly, two Endevco Model 8507C piezoresistive pressure transducers were flush mounted on the upper and lower walls, shown in Fig.5. The transducers are located at a distance of 63.5 mm from the throat on the centerline of each wall. This position is ideal for examining the shock behavior in the cases where significant plume instability was observed. The transducers are housed in a 2.34 mm cylindrical case and have a pressure range of 0-100 kPa.

In addition to the Endevco pressure transducers, each wall of the nozzle is fitted with 24 equally spaced pressure ports extending from an area ratio $A/A_t = 1.14$ upstream of the nozzle throat to the nozzle exit. The 0.8 mm-diameter ports were scanned by a mechanical pressure multiplexer (Scanivalve, Model SSS-48), which consists of a pneumatic selector switch connected to a single pressure transducer (Setra, Model 280). This measurement gives the time-averaged wall pressure distribution over the entire nozzle. Such distributions in this facility have been published in the past[11], so they will not be repeated here. For the present experiments, the mean wall pressure measurements are used to identify the wall with the larger separation zone. It was shown in earlier studies that the pressure recovery on the wall with large separation zone has a distinctive linear rise, whereas on the wall with small

separation zone the pressure shows a faster initial rise followed by a gradual recovery to ambient value11. This trend has also been observed in computations of nozzle flow separation[12].

In conjunction with the wall pressure measurements it was desired to have time resolved measurements of the plume fluctuations. This provided a means of quantifying the instability in the plume as well as correlating the fluctuations to the unsteady internal phenomena. A dynamic Pitot probe (DPP), using an Endevco Model 8507C piezoresistive transducer, was designed to provide time-resolved measurements of the plume impact pressure while minimizing flow intrusion. Originally the transducer was mounted at the tip of the probe. However, the transducer proved vulnerable to dust particles and other impurities in the high-speed stream it was immersed in. As a result, it lasted for only a few measurements and was destroyed by collisions with the small particles. The solution to this persistent problem was the mounting of an S-shaped inlet in front of the transducer, as shown in Fig.6. The inlet prevented a direct "line of sight" of the transducer face with the flow, thus avoiding collision with particles. The replacement transducer has lasted for hundreds of experiments. The drawback is that the inlet introduces a frequency response that must be accounted for when calculating spectra and fluctuation statistics. The limited number of experiments with the original probe designed enabled us to establish such a correction curve that is applied to the spectra and to the computation of the RMS values from the spectra. Additional experiments to establish the correction curve involved measurements of pressure fluctuation inside a cavity, with the S-shaped inlet on and off. The diameter of the inlet is 2.5 mm.

Figure 6 provides a guide for the nomenclature to be used in the rest of the paper. Subscripts 1, 2, and 3 will indicate the time-resolved pressure measurements at the lower wall, upper wall, and dynamic pitot probe, respectively. In cases where separation is asymmetric, the "upper wall" will always be associated with the large separation region and the "lower wall" will be associated with the small separation region.

C. Data processing

For each experimental run, the two wall pressure transducers and the DPP transducer were sampled simultaneously at a sampling rate of 100 kHz for a duration of 1 s. The Nyquist frequency is thus 50 kHz, but avoidance of the transducer resonances sets the useful frequency limit to 30 kHz. A low-pass filter, set at 30 KHz, was thus applied to the signal acquisition. In the discussion that follows, subscripts i and j take the values of 1,2, and 3, corresponding to the signals from the lower wall, upper wall, and DPP, respectively (Fig.6). Denoting by $p_i(t)$ the calibrated output of transducer i, basic statistics include the mean $\overline{p}_i$, standard deviation σ^2_i and root mean square $p_{i,rms} = \sigma_i$. Auto-correlations or cross-correlations are presented in the normalized form

$$R_{ij}(\tau) = \frac{\left\langle p_i(t)\, p_j(t+\tau) \right\rangle}{\sigma_i \sigma_j}$$

where <> denotes the time average. Auto-spectra $S_{ii}(f)$ and cross-spectra $S_{ij}(f)$were computed using a Fast Fourier Transform with 2048 points, giving a frequency resolution of 97 Hz. The coherence between signals i and j is defined as

$$C_{ij}(f) = \frac{S^2_{ij}(f)}{S_{ii}(f) S_{jj}(f)}$$

To account for the non-flat frequency response of the DPP, the variable of the DPP signal is obtained by integration of its auto-spectrum

$$\sigma_3^2 = \int_0^{30kHz} S_{33}(f) e^{i2\pi f}\, df$$

where the upper limit of the integral indicates the highest resolved frequency. In the presentation of the results, time and frequency are non-dimensionalized by the parameter U_e/h_e, where U_e is the ideally-expanded velocity for a given nozzle pressure ratio and h_e is the exit height of the nozzle.

III. Results

A. Plume Pitot Pressure

A parametric investigation of the jet plume versus nozzle shape and pressure ratio has shown significant increase in turbulence fluctuations levels as the exit-to-throat area ratio increases. The fluctuations are quantified in terms of the pressure p_3 measured by the dynamic Pitot probe (DPP), which for the experiments discussed here equals the local total pressure p_0. Figure 7 shows the distribution of $p_{3,\mathrm{rms}}$ a short distance from the nozzle exit and the three-fold increase in rms fluctuation levels as the nozzle area ratio changes from A_e/A_t=1 (straight) to A_e/A_t=1.6 (converging-diverging). Figure 8 shows the corresponding spectra for the peak rms values. We note a substantial increase in the spectral levels at low and moderate frequencies, and little or no increase at high frequencies. The increase in rms levels is consistent with the instability observed in visualizations such as Fig. 1.

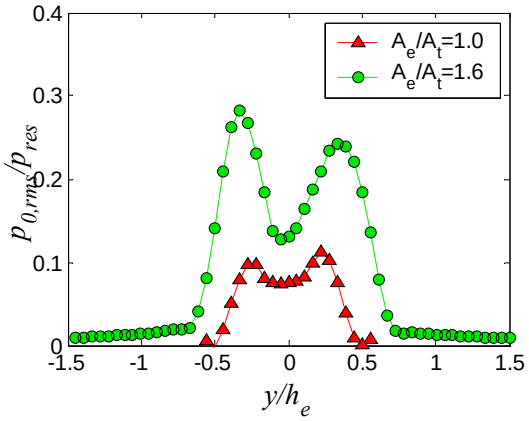

Fig.7 RMS total pressure profile of jet plme at x/h_e=0.5 for straight nozzle (A_e/A_t=1) and convergent-divergent nozzle (A_e/A_t=1.6)

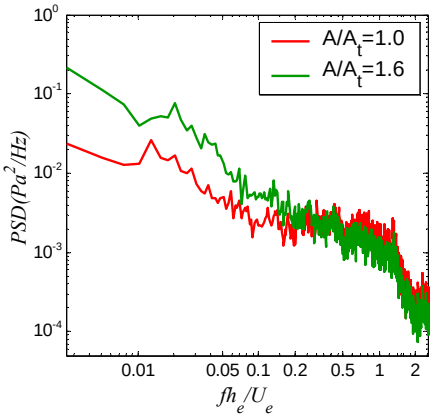

Fig.8 Total pressure spectra associated with the peak RMS levels of Fig.7

B. Wall Pressure Statistics

Before attempting correlations of the shock motion with plume fluctuations, it is helpful to understand the behavior of the oscillating shock as well as the nature of the unsteady flow in its vicinity. To measure the fluctuations in the entire neighborhood of the shock, the nozzle was held at a fixed area ratio of A_e/A_t=1.6 and the nozzle pressure ratio was gradually increased pushing the shock from upstream to downstream of the wall transducers. Figure 9 shows the variation of $p_{1,rms}$ with nozzle pressure ratio. The resulting curve shows the relative magnitude of the wall pressure fluctuations in the various regions around the shock. At higher NPR, corresponding to when the wall transducers are measuring the attached boundary layer upstream of the shock, the fluctuations are comparatively small in magnitude. At the nozzle pressure ratio where the shock begins to influence the pressure transducer, there is a steep increase in $p_{1,rms}$ as a consequence of the large pressure jump across the shock. At lower nozzle pressure ratios, where the transducers are located in the separated region, the fluctuations are larger than in the attached boundary layer but significantly smaller than when the shock is over the transducer.

Figure 10 plots the spectra corresponding to the three regimes of Fig.9. The spectrum of the fluctuations in the attached boundary layer is significantly lower in intensity than the spectra in the two other regimes. It is reasonable to assume that the attached boundary layer plays little or no role on the shock motion. The spectral levels in the separated region are substantial and match those of the shock motion for fh_e/U_e>0.3. Therefore, the fluctuations in the separation zone are likely to have an effect on the shock motion. The spectra of Fig. 10 are similar to the corresponding spectra of shock-boundary layer separation in front of a wedge, as studied by Plotkin[13]. One key aspect of the shock spectrum is that the majority of the fluctuating energy is at very low frequencies. The fact that the shock oscillates at low frequencies, comparable to the low frequencies of the instabilities observed in the plume, foreshadows a possible correlation.

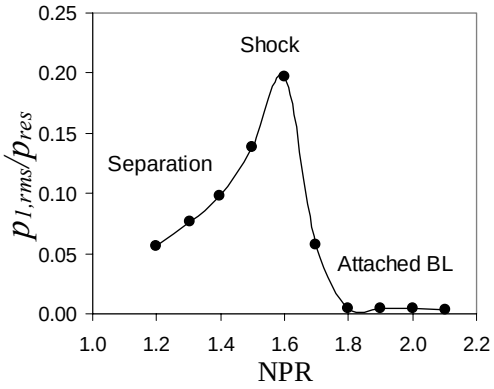

Fig.9 RMS wall static pressure fluctuation versus nozzle pressure ratio, showing different flow regimes.

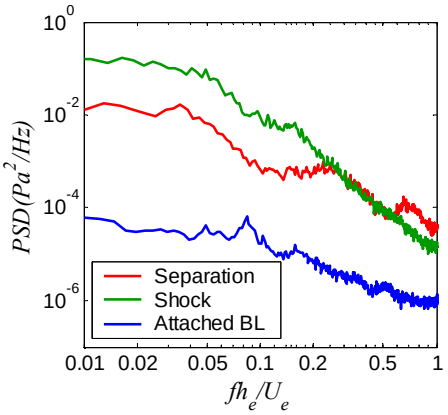

Fig.10 Autospectra of wall static pressure corresponding to the various flow regimes.

C. Correlations between Wall Pressure Ports

The cross correlation and coherence of the two wall transducers illuminate some important characteristics of the unsteady phenomena in supersonic nozzle flow separation. Figures 11 and 12 show the cross correlation and coherence, respectively, of the two wall transducers situated upstream, downstream and at the location of the shock. As one might expect, in the attached boundary layer there is no correlation between the upper and lower wall since the fluctuations are a result of random turbulent eddies. There is a significant correlation when measuring the shock itself, implying that the shock oscillates in a "piston-like" manner. The coherence plot confirms the relatively low frequency of the shock motion.

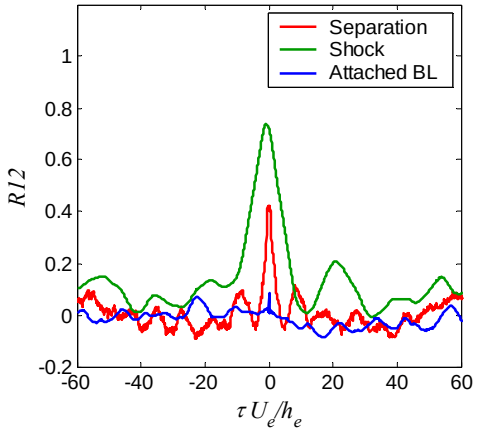

Fig.11 Cross correlations of upper and lower wall transducers for various flow regimes.

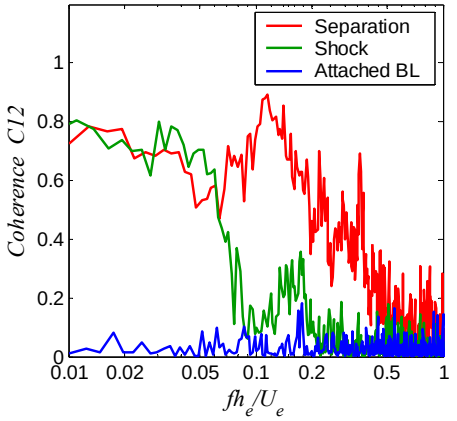

Fig.12 Coherence of upper and lower wall transducers for various flow regimes.

D. Correlations between Wall Pressure Ports and Dynamic Pitot Probe

Several experiments were conducted at area ratio A_e/A_t=1.6, taking simultaneous measurements of the DPP and the wall mounted transducers. Initially the DPP was held at fixed positions in both the large and small separation zones and the nozzle pressure ratio was varied. Later the NPR was fixed at 1.6 and the DPP was translated along certain paths inside and outside the nozzle.

For studying the effect of NPR on the coherence between wall pressures and DPP, we consider the case of the DPP being situated near the upper wall where the large separation zone occurs for NPR>1.4. Figure 13 plots the coherences for NPR=1.2 and 1.6. For NPR=1.2, separation occurs fairly symmetrically and the wall probes are in the separated region. There is no significant coherence between the DPP and either of the wall probes. At NPR=1.6, the shock sits over the wall probes and separation is asymmetric. We observe significant coherence

between the DPP and the wall probes, the coherence between the DPP and lower wall (small separation zone) exceeding the coherence between the DPP and upper wall (large separation zone) at low frequencies. The coherences drop when the NPR increases further, pushing the shock downstream and locating the wall probes in the attached region. This experiment suggests that the best correlations between wall probes and DPP occur when the shock sits in the vicinity of the wall probes. It also suggests that asymmetric separation may amplify those correlations, although this is still speculative. Figure 13 also plots the coherence between the two wall probes, which remains large as the shock moves upstream of the probes.

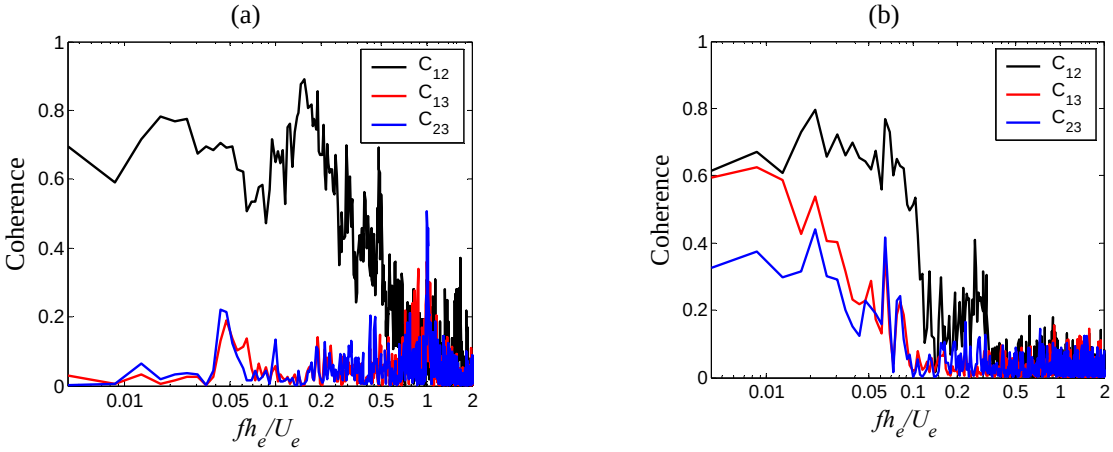

Fig.13 Coherence between upper and lower walls (C_{12}), DPP and lower wall (C_{13}), and DPP and upper wall (C_{23}). (a) NPR=1.2; (b) NPR=1.6.

Having established that the best correlations between wall probes and DPP occur for NPR=1.6 (shock sits over wall ports), the next step was to conduct a search for the locations of DPP where the correlations were maximized. The search pattern is shown in Fig. 14. For a rapid assessment of the trends of the correlations versus DPP position, we plot in Fig. 15 the peak cross-correlations R_{13max} and R_{23max} along the DPP translation paths of Fig. 14. Close to the shock, the correlations peak when the DPP is in the large separation zone (upper wall). There is consistently better correlation of DPP with the lower wall probe that with the upper wall probe. As we exit the nozzle, the DPP remains significantly correlated with the wall probes, and this correlation becomes rather insensitive with the transverse position of the DPP. This is probably because the instability excites the entire plume so it does not matter where the DPP sits. Interestingly, the better correlation of the DPP with the lower wall probe persists even as the DPP moves outside the nozzle. This suggests that instability eddies are created through an interaction between the expansion reflected from the smaller lambda foot and the shear layer of the larger separation.

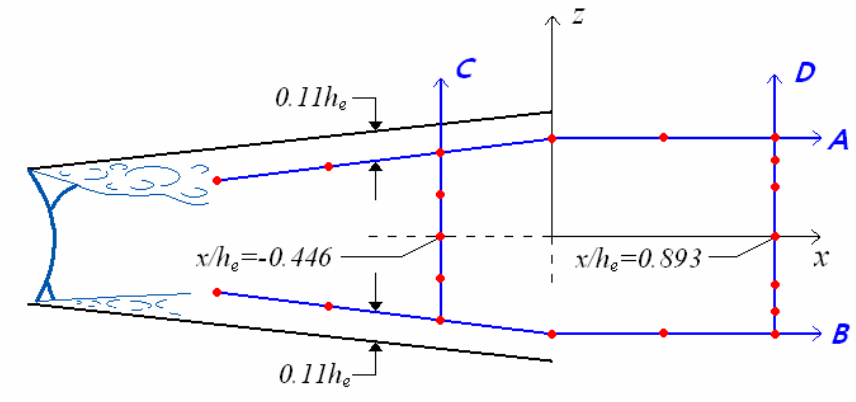

Fig.14 Translation paths of dynamic Pitot probe. Red points indicate measurement locations

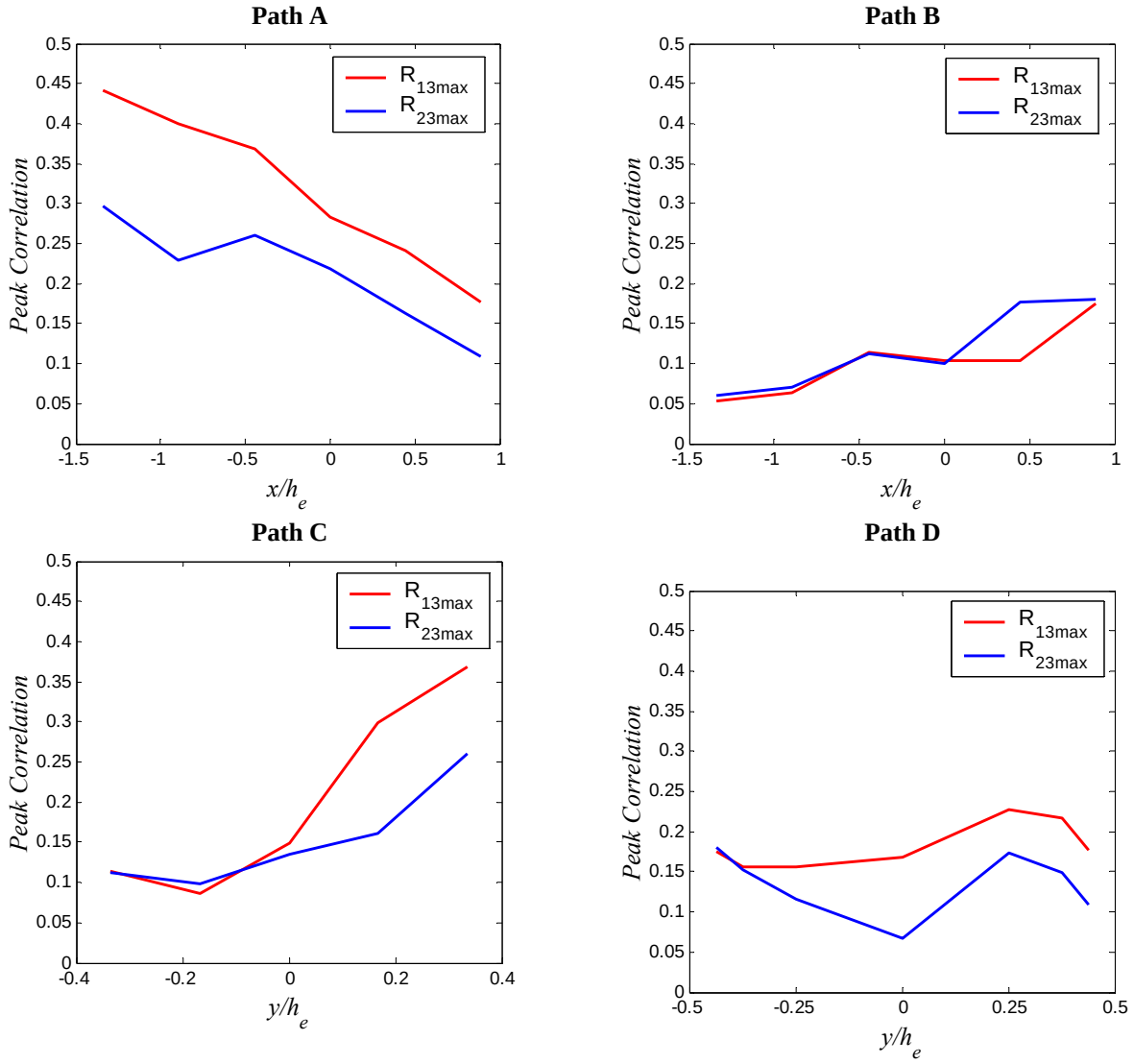

Fig.15 Peak cross-correlactions R_{13max} and R_{23max} for the DPP moving along the paths illustrated in Fig.14

We now provide some further details of the correlations. Figure 16 plots the cross-correlations between DPP and wall pressures with the DPP sitting near the shock in the vicinity of the upper wall (large separation zone). The better correlation with the lower wall pressure is evident. Figure 17 shows the coherences for various positions of the DPP. When the DPP is inside the nozzle and close to the shock, coherences between DPP and wall pressures are substantial when the DPP is in the large separation zone (Fig. 17a) and very small when the DPP is in the small separation zone (Fig. 17b). With the DPP outside the nozzle, the entire plume is unsteady and there is significant coherence between the DPP and the wall probes even when the DPP sits at the centerplane of the jet (Fig. 17c). Looking at the coherence diagrams of Fig. 17 one sees a striking similarity between the motion of the shock, captured by the C_{12} coherence, and the DPP-wall coherences C_{13} and C_{23}. All coherences have similar shapes and occur for non-dimensional frequency below roughly 0.2. This suggests strongly that the plume instability is connected to the shock oscillation. The fact that the coherence between the lower wall pressure (small lambda foot) and the DPP in Fig. 17a is higher than the coherence between the upper and lower wall transducers at very low frequency further suggests that the origin of this instability is a result of a cross-nozzle interaction between the expansion fan from the smaller lambda foot and the shear layer of the large separation zone.

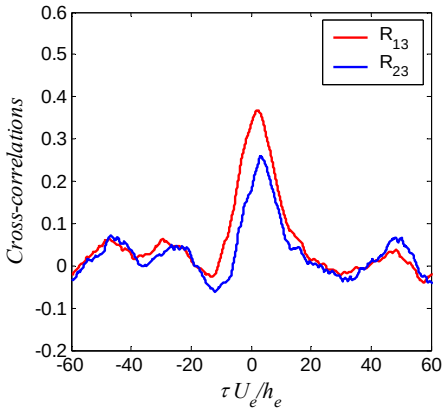

Fig.16 One of strongest cross-correlations between DPP and lower wall (R_{13}), and DPP and upper wall (R_{23}). NPR=1.6.

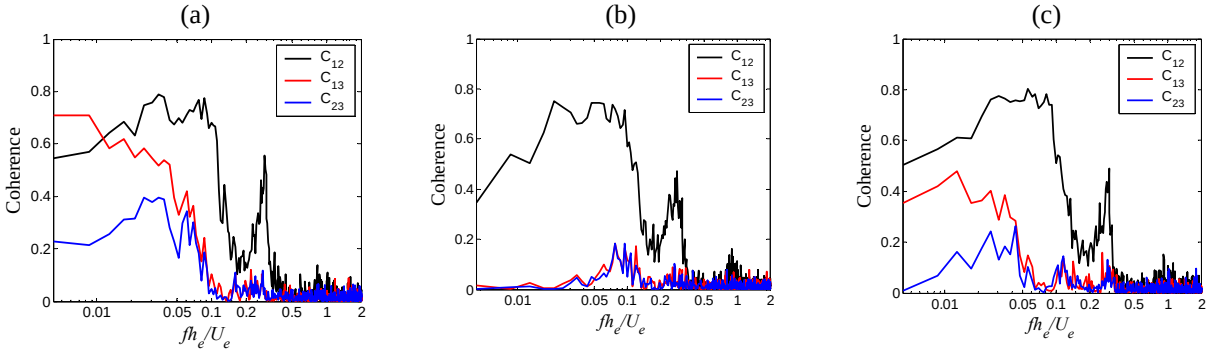

Fig.17 Coherence between upper and lower walls (C_{12}), DPP and lower wall (C_{13}), and DPP and upper wall (C_{23}). NPR=1.6. (a) DPP in large separation zone inside nozzle; (b) DPP in small separation zone inside nozzle; (d) DPP in plume at upper nozzle lip line.

IV. Conclusions

An investigation has been conducted into the source of plume instability from overexpanded convergent-divergent nozzles. The effect of internal shock phenomena on the plume unsteadiness was a particular focus. Time-resolved measurements of wall static pressures and total pressure in the plume were correlated. A summary of the key findings is as follows:

- For nozzle pressure ratios that give rise to shock formation inside the nozzle, increasing the nozzle area ratio from 1 (straight nozzle) to 1.6 (convergent-divergent nozzle) results in a three-fold increase in the rms total pressure fluctuations near the nozzle exit. Spectra indicate that most of the instability energy is contained at low to moderate frequencies.
- For the conditions of this study, the separation shock is asymmetric. This gives rise to a large separation region on one wall and a small separation region on the other wall.
- The coherence and cross correlation of pressures measured on the upper and lower nozzle walls indicate that the shock oscillates in a piston-like manner with no noticeable rotational motion. The oscillation is a low-frequency phenomenon without any resonant tones.
- There are substantial correlations between the wall pressures caused by the shock motion and the total pressure inside the large separation zone. The frequency content of the total pressure fluctuation is similar to that of the shock motion.
- There is consistently better coherence between the total pressure in the large separation zone and the pressure on the wall opposite that zone. This suggests that the instability mechanism is due to an interaction between the expansion fan reflected from the smaller lambda foot with the shear layer of the larger separation zone. This proposed mechanism is shown in Fig.18.

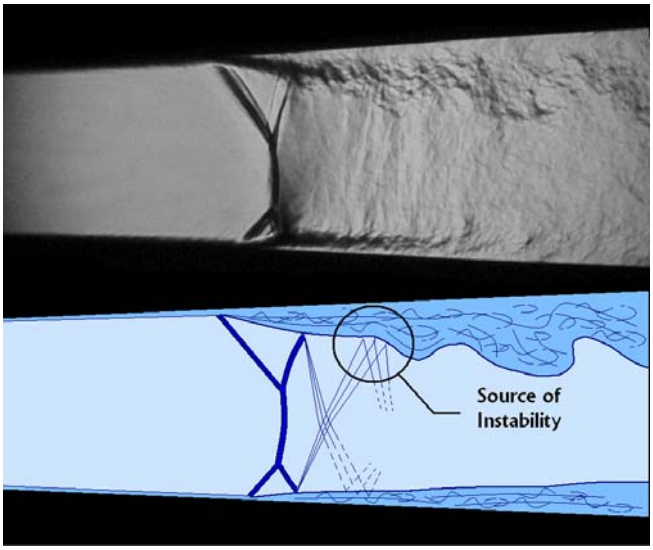

Fig.18 Proposed mechanism of enhancement of shear layer instability.

Acknowledgments

The support from the National University of Singapore, Temasek Labs, is gratefully acknowledged. We thank Prof. Dennis K. McLaughlin (Penn State) for his valuable insights.

References

1. Papamoschou, D., "Mixing Enhancement Using Axial Flow," AIAA Paper 2000-0093, Jan 2000.
2. Murakami,E. and Papamoschou, D., "Experiments on Mixing Enhancement in Dual-Stream Jets," AIAA Paper 2001-0668, Jan. 2001.
3. Papamoschou, D., Dixon, T.D., and Nishi, K., "Mean Flow of Multi-Stream Rectangular Jets under Normal and Mixing-Enhancement Conditions", AIAA Paper 2004-0919, Jan. 2004.
4. Zaman, K.B.M.Q, and Papamoschou, D., "Study of Mixing Enhancement Observed with a Co-Annular Nozzle Configuration," AIAA Paper 2000-0094, Jan. 2000.
5. Morrisette, E.L., and Goldberg, T.J., "Turbulent Flow Separation Criteria for Overexpanded Supersonic Nozzles," NASA TP 1207, Aug. 1978.
6. Wilmoth, R.G., and Leavitt, L.D., "Navier Stokes Predictions of Multifunction Nozzle Flows," *Society of Automotive Engineers Transactions*, Vol. 96, Sec.6, Paper 871753, 1987, pp. 6.865-6.879.
7. Hamed, A., and Vogiatzis, C., "Overexpanded Two-Dimensional Convergent-Divergent Nozzle Flow Simulations, Assessment of Turbulence Models," *Journal of Propulsion and Power*, Vol. 13, No. 3, 1997, pp. 444-445.
8. Hunter, C.A., "Experimental, Theoretical and Computational Investigation of Separated Nozzle Flows," AIAA Paper 98-3107, Jan. 1998.
9. Romine, G.L.,"Nozzle Flow Separation," *AIAA Journal*, Vol. 36, No.9, 1998, pp. 1618-1625.
10. Zaman, K.B.M.Q., Dahl, M.D., Bencic, T.J., and Loh, C.Y., "Investigation of a Transonic Resonance with Convergent-Divergent Nozzles," *Journal of Fluid Mechanics*, Vol. 263, 2002, pp. 313-343.
11. Papamoschou, D., Zill, A., "Fundamental Investigation of Supersonic Nozzle Flow Separation," AIAA Paper 2004-1111.
12. Xiao, Q., Tsai, H.M., and Papamoschou, D., "Numerical Investigation of Supersonic Nozzle Flow Separation," AIAA Paper 2005-4640, June 2005.
13. Plotkin, K.J., "Shock Wave Oscillation Driven by Turbulent Boundary-Layer Fluctuations," *AIAA Journal*, Vol. 13, No. 8, 1975, pp. 1036-1040.